Density Functional Theory Study of Hydrogen Adsorption on $Fe_5C_2(001)$, $Fe_5C_2(110)$, and $Fe_5C_2(100)$

Dong-Bo Cao,[†] Fu-Qiang Zhang,[†] Yong-Wang Li,[†] Jianguo Wang,[†] and Haijun Jiao*[,†,‡]

State Key Laboratory of Coal Conversion, Institute of Coal Chemistry, Chinese Academy of Sciences, Taiyuan 030001, People's Republic of China, and Leibniz-Institut für Organische Katalyse an der Universität Rostock e.V., Buchbinderstrasse 5-6, 18055 Rostock, Germany

Received: August 20, 2004; In Final Form: October 28, 2004

Density functional theory calculations have been carried out for hydrogen adsorption on the (001), (110), and (100) surfaces of Fe_5C_2. At 1/3 and 2/3 monolyer (ML) on (001), the most stable hydrocarbon species is C_sH, while C_sH and C_sH_3 can coexist at 1 ML. On (110), only dissociated hydrogen is found at 2/5 ML, while C_sH is the most stable hydrogen carbon species at 4/5 ML, and C_sH and CH_3 coexist at 6/5 ML. On (001) and (110) surfaces, C_sH_2 is less stable and can dissociate into C_sH or convert into C_sH_3, respectively. These results are in agreement with the experimental observations. On the metallic $Fe_5C_2(100)$ surface which lacks surface carbon atoms on the surface monolayer, dissociated hydrogen is found at 1/2 ML, while both dissociated hydrogen and activated H_2 are found at 1 ML.

1. Introduction

Hägg iron carbide (Fe_5C_2) is an important active phase in iron-based catalysts in Fischer−Tropsch synthesis (FTS) processes.[1] Iron carbide and iron phases can be transformed into each other under a H_2 or synthesis gas ($CO + H_2$) atmosphere.[2] It is found that the carbon of iron carbide can be reduced to CH_x ($x = 1-3$) fragments and CH_4 as detected by infrared spectroscopy.[2] CH_x fragments have been proposed to be key intermediates in FTS processes,[3] and therefore for the formation of hydrocarbon products.[4] To control and modify these catalytic reactions, a detailed understanding of thermodynamic properties of these intermediates as a function of coverage on various catalyst surfaces is highly desired, but very hard to measure or detect under real working conditions. However, the increasing applicability of modern theoretical methods in various fields of chemistry provides an alternative tool to model and to understand catalytic reactions at the level of molecular chemistry.

Hydrogen adsorption on surfaces of transition metals and transition-metal carbides have widely been studied due to their importance in heterogeneous catalysis and hydrogen corrosion, resulting in a dramatic decrease in plasticity and drastic degrading of mechanical properties.[5−7] Experimental and density functional theory (DFT) studies of hydrogen adsorption on Fe(110),[8] Pd(111),[9] and Ru(0001)[10] indicate that hydrogen prefers to adsorb on a 3-fold site. Klinke et al.[11] investigated hydrogen adsorption on Ni(111) and Co(0001) surfaces using DFT methods, and found that the most stable adsorbed sites at 1/2 and 1 monolayer (ML) coverage are 3-fold sites. Using angle-resolved photoemission spectroscopy, Bradshaw et al.[12] studied hydrogen adsorption on TiC(111) and found that the hydrogen-induced state appears below the Fermi level by −6.8 eV. Using high-resolution electron energy loss spectroscopy, Aizawa et al.[13] studied hydrogen adsorption on the surfaces of MC(111), with M = Ti, Zr, Hf, Nb, and Ta, and found that hydrogen (deuterium) is adsorbed dissociatively and the adsorption sites are 3-fold sites on the basis of frequency analysis for M = Ti, Zr, Hf, and Nb, while a different mode on TaC(111) was suspected to have interaction between hydrogen and surface carbon.

For the processes of hydrogen-reduced Fe_5C_2, coexistence of various species (H_2, H, CH_x ($x = 1-3$) fragments, and CH_4) on the surface is possible. The thermodynamic stability of CH_x fragments on transition-metal surfaces has widely been studied both experimentally and theoretically. Stockwell et al. studied the mechanism of FTS on Fe/TiO_2 and Fe/Al_2O_3 catalyst, and found CH as being the major CH_x species by CO/D_2 and $^{13}CO/H_2$.[4b] Among CH_x adsorbed, CH is the most stable species on Ru(0001) as found experimentally and theoretically.[14,15] Petersen et al. studied the chemisorption of CH_4 and its dissociated intermediates, and found CH to be the most stable intermediate on Pt(110) on the basis of DFT calculations,[16] and this finding agrees with the molecular beam experiments by Watson et al.[17]

Despite the importance of reduction of iron carbide surfaces by hydrogen, the corresponding theoretical studies are totally lacking. In this paper, we present extensive calculations of hydrogen adsorption on $Fe_5C_2(001)$, -(110), and -(100) at different coverages, especially the thermodynamic properties of the coexisting species on the surface, e.g., H_2, atomic hydrogen, CH_x ($x = 1-3$) fragments, and CH_4. Thermodynamic studies can provide the adsorption energies and geometry of various surface species at different coverages, which determine their relative stability. These results are compared with the available experimental data. To understand the nature of the bonding of CH_x fragments on (001) and (110), detailed analyses of electronic structure with the local density of states (LDOS) were carried out.

* To whom correspondence should be addressed. E-mail: hjiao@ifok.uni-rostock.de.

[†] Chinese Academy of Sciences.

[‡] Leibniz-Institut für Organische Katalyse an der Universität Rostock e.V.

10.1021/jp046239+ CCC: $30.25
Published on Web 12/21/2004

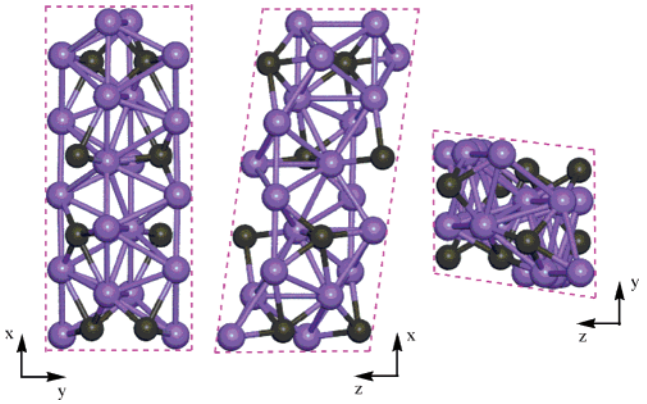

Figure 1. Schematic unit cell of Fe_5C_2 (purple, Fe atom; gray, C atom).

2. Methods and Models

Density functional theory calculations within the generalized gradient approximation (GGA)[18] were carried out to study hydrogen adsorption on the surfaces of Fe_5C_2. All calculations were carried out by using the Cambridge sequential total energy package (CASTEP).[19] Ionic cores were described by the ultrasoft pseudopotential,[20] and the Kohn−Sham one-electron states were expanded in a plane wave basis set up to 340 eV. The error of the adsorption energy at the level of cutoff between 300 and 340 eV was about 0.02 eV. A Fermi smearing of 0.1 eV was utilized. Brillouin zone integration was approximated by a sum over special *k*-points chosen using the Monhorst−Pack scheme.[21] The pseudopotential with a partial core was used in spin-polarized calculations to include nonlinear core corrections.[22] Spin polarization having a major effect on the adsorption energies for a magnetic system[23] was included for the super-paramagnetic Fe_5C_2[24] to correctly account for its magnetic properties. Spin polarization was also used to calculate the energy and structural parameters of the isolated CH_x ($x = 1-3$) species. Without counting the adsorbate, the vacuum between the slabs was set to span in the range of 10 Å to ensure no significant interaction between the slabs. The convergence criteria for structure optimization and energy calculation were set to (a) SCF tolerance of 2.0×10^{-6} eV/atom, (b) energy tolerance of 2.0×10^{-5} eV/atom, (c) maximum force tolerance of 0.05 eV/Å, and (d) maximum displacement tolerance of 2.0×10^{-3} Å. We used the Molarch$^+$ program[25] to generate the molecular graphics.

TABLE 1: Computed Bond Lengths (*d*, Å) and Adsorption Energies (E_{ads}, eV) for Hydrogen Adsorption on Fe_5C_2(001) at 1/3 ML

	1	2	3	4	5
d_{H-H}	0.855				
d_{H-Fe}	1.710	1.616	1.738	1.723	1.811
	1.703	1.731	1.760	1.811	
		1.636	1.845	1.816	
		1.866	1.614		
			1.693		
			2.065		
d_{H-Cs}				1.097	1.119
					1.157
E_{ads}	−0.42	−0.73	−0.90	−1.56	−0.75

Hägg iron carbide (Fe_5C_2) has a monoclinic unit cell (a = 11.5620 Å, b = 4.5727 Å, c = 5.0595 Å, and β = 97.74°),[26] as shown in Figure 1. In our previous work,[27] the optimized unit cell parameters agree with experiment (a = 11.5007 Å, b = 4.4789 Å, c = 4.9536 Å, and β = 97.63°). For the three surfaces of Fe_5C_2, (001), (110), and (100) created from the Fe_5C_2 crystal structure, the geometric and energetic differences between the bare and optimized structures are small and reveal the quality of the employed theoretical methods. Note that the surface structures and compositions of FTS catalysts under the real reaction conditions are unknown experimentally. However, it has been well proved that iron-based FTS catalysts undergo continuous phase transformation from their original phase Fe_2O_3 as prepared during reduction and from those formed in reduction during FTS reaction.[28−31] In our calculations, the initial parameters of H_2 atop the iron atoms were set to 1.75 Å for H−Fe (from low-energy electronic diffraction[32]) and those for the surface carbon (C_s−H) were 1.25 Å, while the H−H distance was 0.75 Å.

For the front view of Fe_5C_2(001), we used a model system with five iron layers and three carbon layers (5Fe/3C), in which the bottom two iron layers and two carbon layers (2Fe/2C) were fixed in their bulk positions, while the three iron layers and

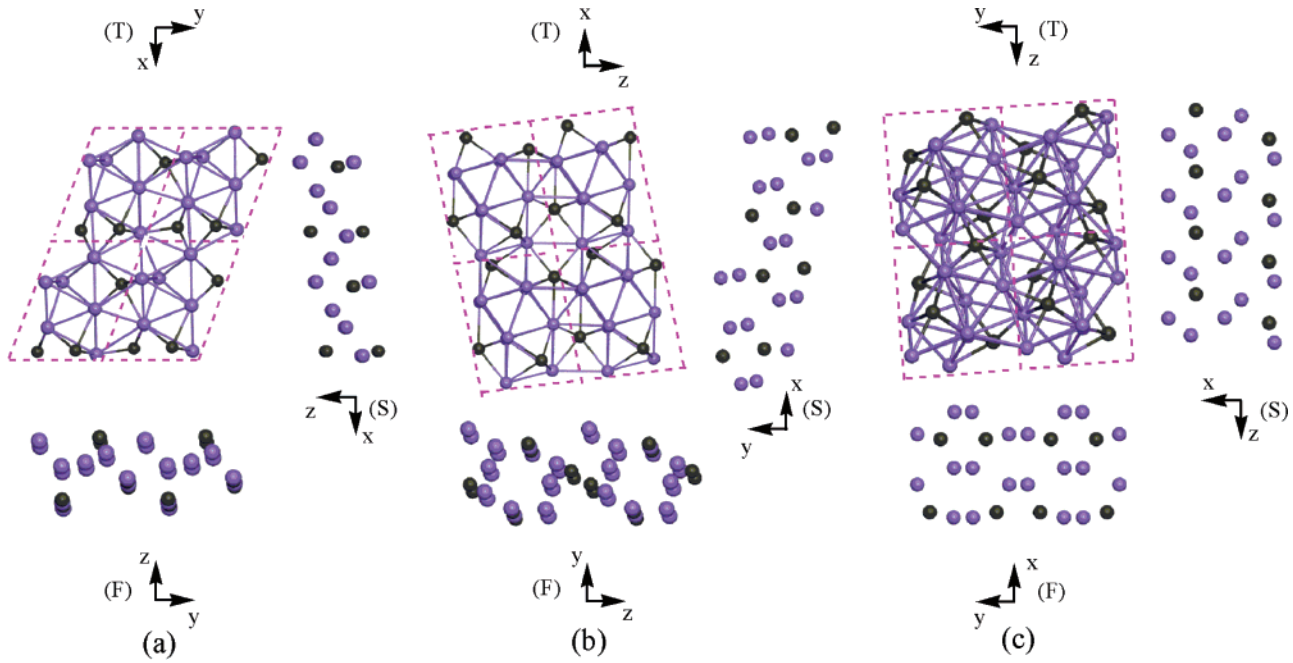

Figure 2. Schematic top (T), front (F), and side (S) views of the (001) (a), (110) (b), and (100) (c) surfaces in a p(1 × 1) unit cell of Fe_5C_2.

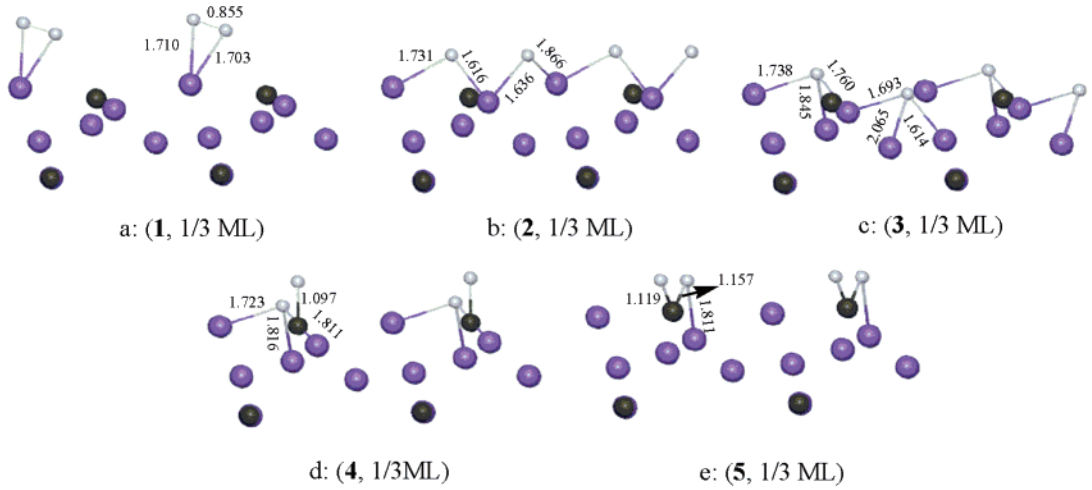

Figure 3. H adsorption on Fe_5C_2(001) at 1/3 ML (purple, Fe atom; gray, C atom; white, H atom).

TABLE 2: Computed Bond Lengths (*d*, Å) and Adsorption Energies (E_{ads}, eV) for Hydrogen Adsorption on Fe_5C_2(001) at 2/3 ML

	6	7	8	9	10	11	12	13	14
d_{H-H}	0.833			0.867					
d_{H-Fe}	1.705	1.650	1.649	1.737	1.680	1.624	1.723	1.700	
	1.775	1.684	1.674	1.686	1.749	1.727	1.763	1.748	
	1.803	1.753	1.668	1.711	1.902	1.649	1.807	1.834	
	1.736	1.765	1.685		1.665	1.684			
	1.744	1.690	1.717		1.674	1.747			
		1.713	1.722		1.858	1.826			
		1.885	1.689						
			1.719						
			1.948						
d_{H-Cs}	1.097	1.091		1.112	1.105	1.102	1.090	1.089	1.090
				1.184	1.205	1.206	1.111	1.090	1.090
							1.118	1.095	1.091
									1.093
E_{ads}	−0.93	−0.97	−0.50	−0.59	−0.80	−0.78	−0.67	−0.47	−0.68 (−0.02)[a]

[a] Using CH_4 as absorbate.

one carbon layer on the top (3Fe/1C) were allowed to relax (Figure 2a). The top layer of Fe_5C_2(001) has both Fe and C, and their ratio is 1:1, while the second and third layers contain only Fe atoms. A 3 × 5 × 2 *k*-grid sampling within the Brillouin zones was used in the p(1 × 1) unit cell. We also tested the *k*-point sampling by using the 4 × 6 × 2 Monkhorst−Pack meshes for the unit cell, and the change in energy is less than 0.02 eV. For checking the influence of the thickness, we also performed calculations on a model system with seven iron layers and three carbon layers (7Fe/3C) under the relaxation of the top four iron layers and two carbon layers (4Fe/2C), and the change in adsorption energy of **1**−**4** is less than 0.19 eV, except the large change of that (0.44 eV) of **5** in which surface C_sH_2 is formed.

For the front view of Fe_5C_2(110), a slab consisting of six iron layers and four carbon layers (6Fe/4C) with a p(1 × 1) surface unit cell was modeled (Figure 2b). The top layer is composed of Fe atoms, while the ratio of Fe and C is 2:1 on the second and third layers, and the carbon atoms of the second layer are exposed and have an open-surface structure. In the calculations, the bottom three iron layers and two carbon layers (3Fe/2C) were fixed in their bulk positions, while the top three iron layers and two carbon layers (3Fe/2C) were allowed to relax. A *k*-point sampling was performed using 4 × 3 × 1 Monkhorst−Pack meshes for the unit cell. Comparison with the energy of the 5 × 4 × 2 Monkhorst−Pack meshes for the unit cell, the error is less than 0.01 eV. It is found that a slab of five iron layers and three carbon layers (5Fe/3C) under the relaxation of the top three iron layers and two carbon layers (3Fe/2C) results in energy changes of 0.05, −0.07, 0.19, and −0.07 eV in **24**, **25**, **26**, and **28**, respectively.

For the front view of Fe_5C_2(100), a slab composed of five iron layers and two carbon layers (5Fe/2C) with a p(1 × 1) surface unit cell was modeled (Figure 2c). The top and third layers are consisted only of Fe atoms, while the ratio of Fe and C is 1:1 on the second layer and the carbon atoms are covered or hidden under the top Fe layer. In the calculations, the bottom two iron layers and one carbon layer (2Fe/1C) were fixed in their bulk positions, while the top three iron layers and one carbon layer (3Fe/1C) were allowed to relax. A *k*-point sampling of the 4 × 4 × 1 Monkhorst−Pack meshes for the unit cell was used. Comparison with the energy using the 5 × 5 × 2 Monkhorst−Pack meshes for the unit cell, the error was less than 0.01 eV. With a slab of four iron layers and one carbon layer (4Fe/1C) under the relaxation of the top two iron layers and one carbon layer (2Fe/1C), the changes of adsorption energies in **47**, **48**, and **51** are −0.75, −0.07, and 0.0 eV. The large change in **47** is due to structure **47** being transformed into **48**. We also tested a slab of four iron layers and two carbon layers (4Fe/2C) under the relaxation of the top three iron layers and one carbon layer (3Fe/1C). The changes of adsorption energies in **47**, **48**, and **51** are 0.09, −0.15, and −0.25 eV. Thus, there is no significant effect of the slab thickness in both relaxed and fixed layers on the adsorption energy of all surfaces. This

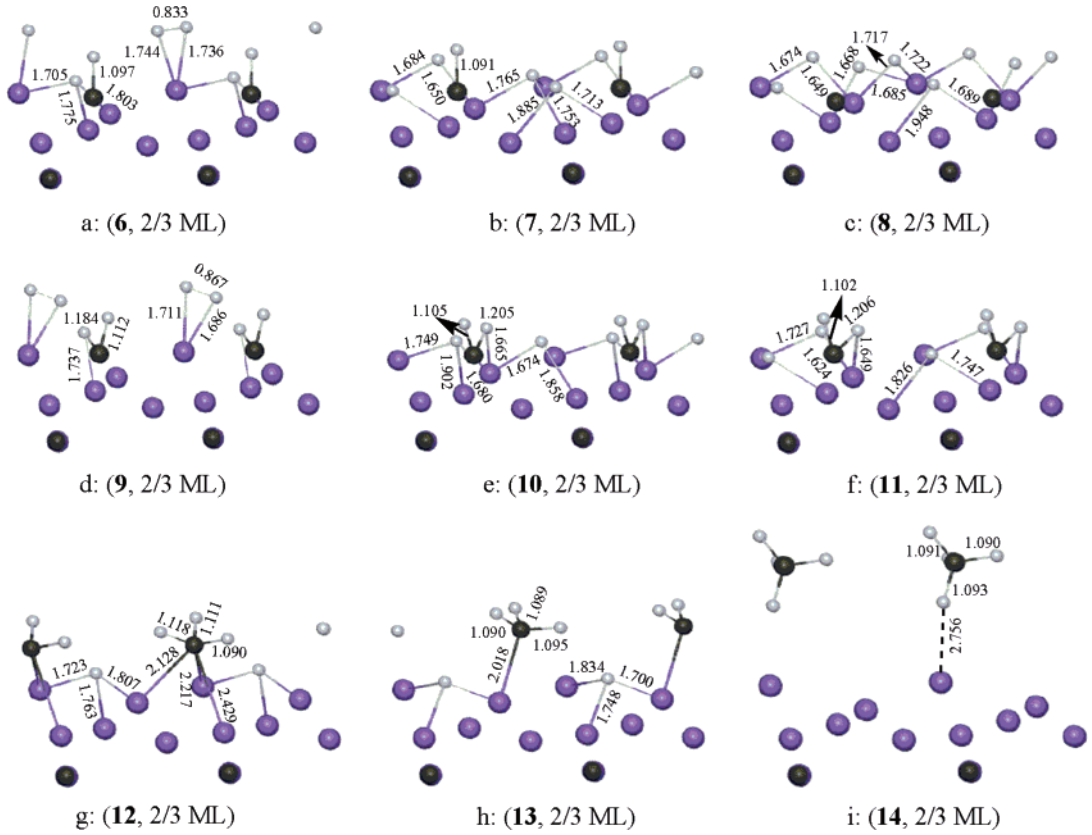

Figure 4. H adsorption on $Fe_5C_2(001)$ at 2/3 ML (purple, Fe atom; gray, C atom; white, H atom).

TABLE 3: Computed Bond Lengths (*d*, Å) and Adsorption Energies (E_{ads}, eV) for Hydrogen Adsorption on $Fe_5C_2(001)$ at 1 ML

	15	16	17	18	19	20	21	22	23
d_{H-H}	0.864	0.843							0.862
d_{H-Fe}	1.590	1.652	1.633	1.719	1.657	1.732	1.714	1.726	1.702
	1.728	1.681	1.679	1.743	1.713	1.800	1.797	1.759	1.716
	1.666	2.053	1.628	1.790	2.005	1.839	1.840	1.806	
	1.893	1.672	1.705	1.672	1.725	1.773	1.696	1.731	
	1.937	1.720	1.704	1.685	1.766	1.829	1.752	1.790	
	1.621	1.721	1.706	1.800	1.788	1.871	1.943	1.827	
	1.638	1.666	1.691	1.724	1.706				
	1.657	1.798	1.699	1.731	1.775				
	1.777	1.805	1.986	1.841	1.840				
	1.923		1.735						
d_{H-Cs}	1.093	1.104	1.090	1.087	1.087	1.088	1.090	1.089	1.089
		1.193	1.190	1.103	1.090	1.090	1.090	1.090	1.090
				1.127	1.094	1.091	1.090	1.090	1.090
						1.093	1.093	1.092	1.092
E_{ads}	−0.79	−0.64	−0.51	−0.79	−0.74	−0.94	−0.90	−0.87	−0.58
						(−0.02)[a]	(−0.02)[a]	(−0.01)[a]	(0.00)[a]

[a] Using CH_4 as adsorbate.

is in agreement with the adsorption of CO molecules on the Fe_5C_2 surfaces.[27]

The adsorption energy per H_2 is defined as $E_{ads} = E(H/slab) - [E(slab) + E(H_2)]$, where the first term is the total energy for the slabs with hydrogen adsorbed on the surface per H_2, the second term is the total energy of the bare slab of the surface, and the third term is the total energy of free H_2. Therefore, the more negative the E_{ads}, the higher the adsorption energy.

3. Results and Discussion

3.1. Hydrogen Adsorption on $Fe_5C_2(001)$. *3.1.1. Adsorption Geometry*. As shown in Figure 3, there are five models (**1**−**5**) for hydrogen adsorption on $Fe_5C_2(001)$ at 1/3 ML, and the computed bond parameters and adsorption energies are given in Table 1. **1** shows the adsorption of H_2 at an atop site, which is activated, but not dissociated, as indicated by the elongated bond length of 0.855 Å, while **2** and **3** show the adsorption of atomic hydrogen (H) at 2-fold and 3-fold sites, respectively. **3** has higher adsorption energy than **1** and **2** (−0.90 vs −0.42 and −0.73 eV). The tendency is in agreement with that of hydrogen adsorption on metal surfaces.[8−11,13]

4 has a 3-fold hydrogen adsorption on iron atoms and a surface C_sH fragment with a C_s-H bond of 1.097 Å, as in the case of CH adsorption on Pt(110),[16] Ni(111), Co(0001),[33] and Ru(0001).[34] **5** has a surface C_sH_2 fragment with C_s-H bond lengths of 1.119 and 1.157 Å. Note that one H of C_sH_2 is agostically bonded with an Fe atom at 1.811 Å. However, **5** has a much lower adsorption energy than **4** (−0.75 vs −1.56

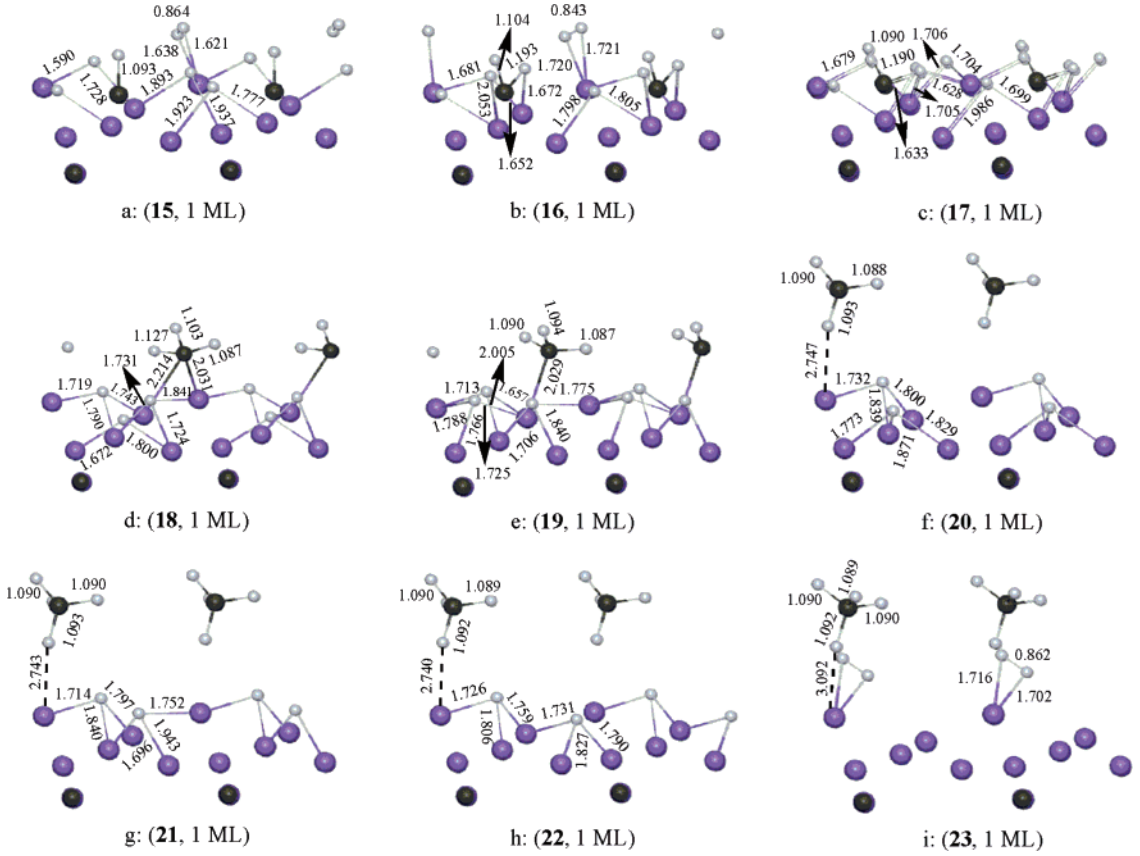

Figure 5. H adsorption on Fe_5C_2(001) at 1 ML (purple, Fe atom; gray, C atom; white, H atom).

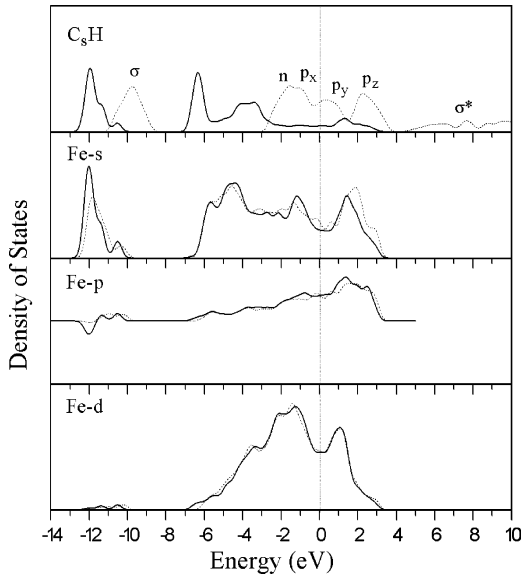

Figure 6. LDOS of the surface C_sH fragment in **4** at 1/3 ML on Fe_5C_2-(001) (solid line for bands after adsorption, dashed line for bands before adsorption).

eV). On this basis, **5** with C_sH_2 should dissociate into **4** with C_sH directly, and **4** should be the only species on Fe_5C_2(001) at 1/3 ML.

For hydrogen on Fe_5C_2(001) at 2/3 ML, there are nine adsorption modes (**6**−**14**), and the calculated bond parameters are given in Table 2 and Figure 4. **6** and **7** with higher adsorption energies (−0.93 and −0.97 eV) than other species have the coexistence of surface species C_sH and H_2/H. In **6**, there are C_sH and H_2 at atop sites and H at 3-fold sites, while **7** has C_sH and H at two 2-fold sites and one 3-fold site. In **8**, there are also adsorbed H species at two 2-fold sites and one 3-fold site, but without formation of a surface C_sH fragment, and the calculated adsorption energy of **8** (−0.50 eV) is much lower than those of **6** and **7**. As compared with **4** at 1/3 ML, the adsorption energies per H_2 for **6** and **7** are lower.

In **9**, there are adsorbed C_sH_2 and H_2, and one H of C_sH_2 is agostically bonded to an iron atom at 1.737 Å. **10** and **11** have coadsorbed C_sH_2 and H species at one 3-fold site and one 2-fold site. The adsorption energies of **10** and **11** are higher than that of **9** (−0.80 and −0.78 vs −0.59 eV).

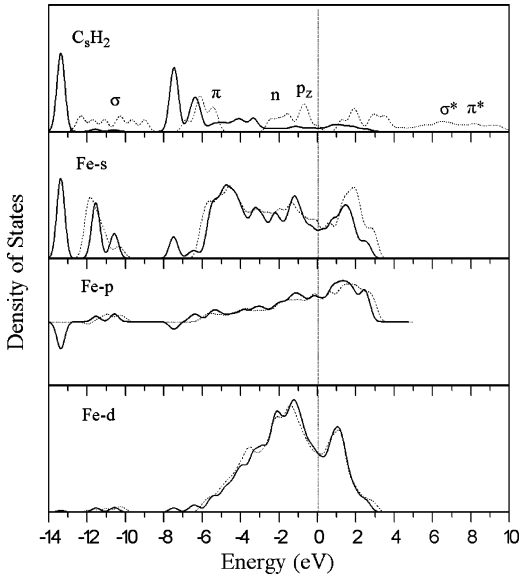

Figure 7. LDOS of the surface C_sH_2 fragment in **5** at 1/3 ML on Fe_5C_2-(001) (solid line for bands after adsorption, dashed line for bands before adsorption).

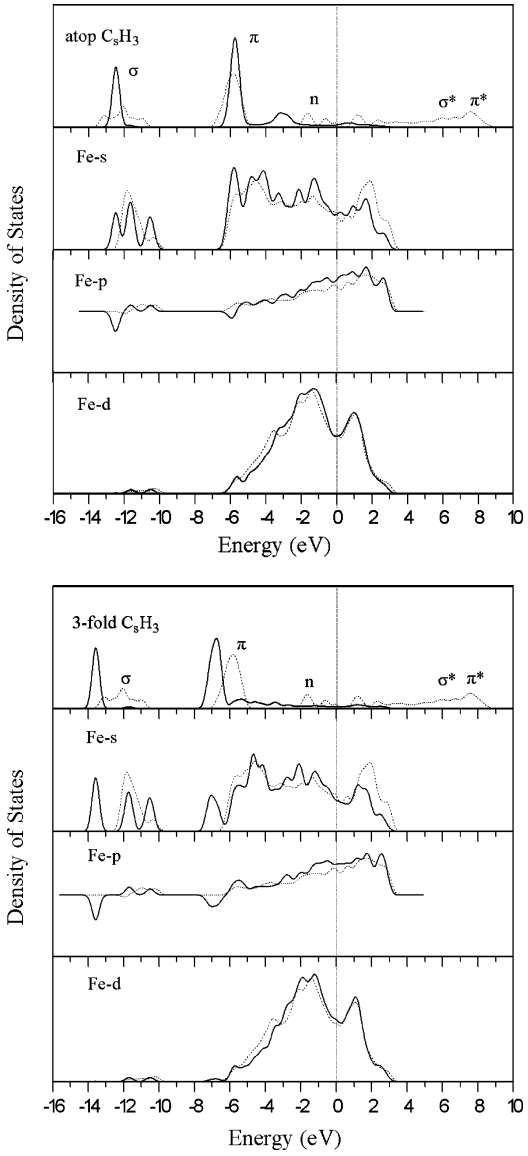

Figure 8. LDOS of the surface C_sH_3 fragment at the atop site in **13** and 3-fold site in **12** at 2/3 ML on $Fe_5C_2(001)$ (solid line for bands after adsorption, dashed line for bands before adsorption).

In **12** and **13**, surface C_sH_3 fragments are formed. However, the adsorption energies of **12**/**13** with C_sH_3 are lower than those of **6**/**7** with C_sH, and **10**/**11** with C_sH_2. In **12**, there are C_sH_3 at a 3-fold site and H at a 3-fold site. In **13**, there are C_sH_3 at atop sites and H adsorbed at 3-fold sites. The adsorption energy of **12** is higher than that of **13** by 0.20 eV. For direct comparison, we calculated the adsorption energy of only C_sH_3 at 3-fold and atop sites as adsorbate, and the 3-fold site is more favored by 0.13 eV. This is in contrast to the tetravalence rule, as suggested by Hoffmann et al.[35] and Somorjai et al.,[36] for the binding of the simplest hydrocarbon fragments on the (111) surfaces of transition metals to complete their tetravalence, e.g., C_sH_3 at atop sites, C_sH_2 at bridge sites, and CH at 3-fold sites on the basis of orbital interactions. However, experimental and theoretical studies suggested that this rule may be violated for certain metals, with the result that CH_3 favors a 3-fold site instead of an atop site on Ni(111),[37] Cu(111),[38] and Ru(0001).[14]

TABLE 4: Computed Bond Lengths (*d*, Å) and Adsorption Energies (E_{ads}, eV) for Hydrogen Adsorption on $Fe_5C_2(110)$ at 2/5 ML

	24	25	26	27	28	29
d_{H-H}	1.018					
d_{H-Fe}	1.602	1.695	1.739	1.739	1.701	1.681
	1.608	1.802	1.757	1.760	1.797	1.737
		1.876	1.804	1.842	1.891	
		1.678	1.684	1.708		
		1.721	1.691	1.793		
				1.826		
d_{H-Cs}					1.114	1.110
E_{ads}	−0.64	−1.17	−1.44	−1.43	−1.16	−1.06

In **14**, surface C_sH_4 is formed with an adsorption energy of −0.68 eV. Considering CH_4 as adsorbate, the adsorption energy of CH_4 in **14**, defined as $E_{ads} = E(CH_4/slab') - [E(slab') + E(CH_4)]$, in which slab′ is the slab excluding the surface carbon atom, is very low (−0.02 eV), and this is in line with the long Fe−H distance of 2.756 Å. This suggests that CH_4 immediately leaves the surfaces once formed, and no CH_4 adsorption is possible on a real catalyst surface in FTS. On the basis of the calculated adsorption energies for H on $Fe_5C_2(001)$ at 2/3 ML, the energetically most favored surface fragment is C_sH (**6**/**7**). This is in agreement with the experimental observation by CO/D_2 and $^{13}CO/H_2$ on Fe/Al_2O_3 during FTS.[4b] This also agrees with the theoretical and experimental results showing CH as the most stable species among CH_x ($x = 1-3$) adsorbed on Ru(0001) and Pt(110) surfaces.[14−17]

For hydrogen on $Fe_5C_2(001)$ at 1 ML, there are nine adsorbed modes (**15**−**23**), and the calculated bond parameters are listed in Table 3 and Figure 5. In **15**, there are C_sH and H_2 at atop sites and H species adsorbed at 2-fold and two 3-fold sites. Surface C_sH_2 is formed in **16** and **17**. In **16**, there are C_sH_2 and

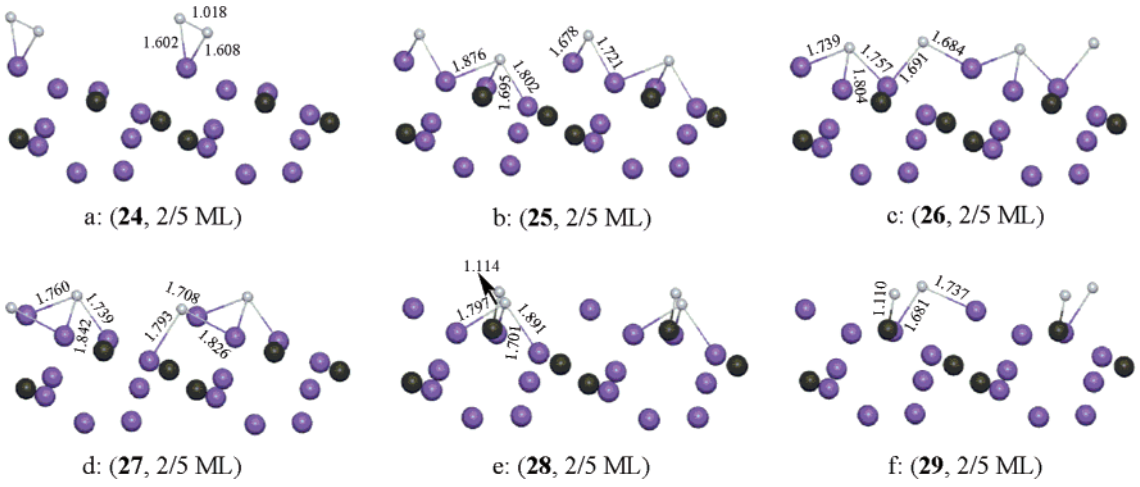

Figure 9. H adsorption on $Fe_5C_2(110)$ at 2/5 ML (purple, Fe atom; gray, C atom; white, H atom).

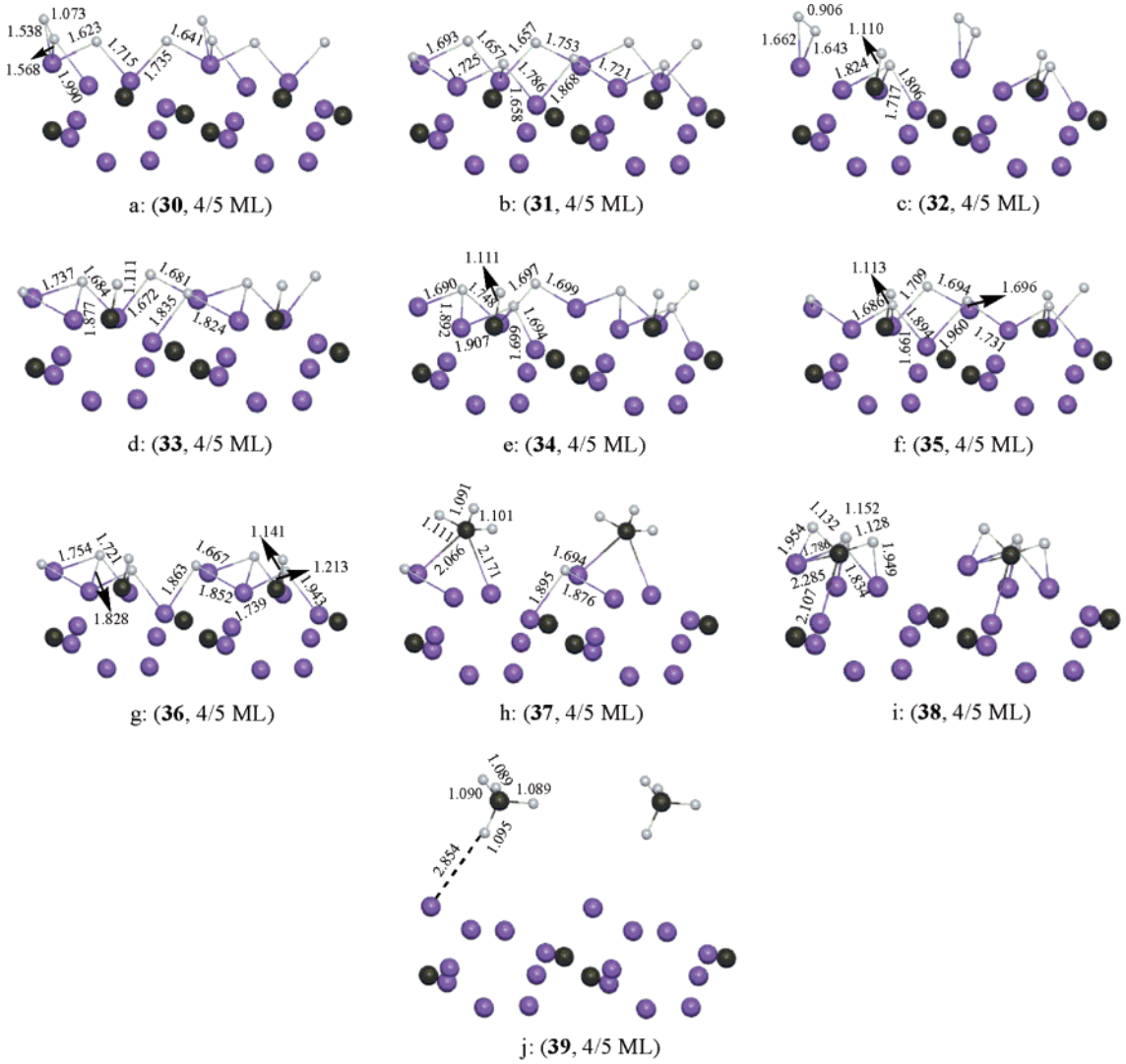

Figure 10. H adsorption on Fe_5C_2(110) at 4/5 ML (purple, Fe atom; gray, C atom; white, H atom).

H_2 at atop sites and H species adsorbed at two 3-fold sites, and one H of C_sH_2 is agostically bonded to an iron atom at 1.672 Å, while in **17** there are C_sH_2 and H adsorbed at three 2-fold sites and one 3-fold site, and one H of C_sH_2 is agostically bonded to an iron atom at 1.735 Å. Both **18** and **19** have surface C_sH_3 fragments and H at 3-fold sites. The adsorption energies of **15** with C_sH and **18**/**19** with C_sH_3 are close (−0.79 vs −0.79/−0.74 eV), but they are higher than those (−0.64/−0.51 eV) of **16**/**17** with C_sH_2, respectively. As in **12**/**13**, the adsorption energy of **18** with one 2-fold C_sH_3 and three 3-fold H species is higher than that of **19** with an atop C_sH_3 and three 3-fold H species.

20−**23** are modes with C_sH_4. In addition to C_sH_4, **20**−**22** have H adsorbed at two 3-fold sites, while **23** has activated H_2 at atop sites. The adsorption energies of **20**−**22** are much higher than those of **23** and **15**−**19** (Table 3). This suggests that C_sH_4 is the most favored species thermodynamically for H adsorption on Fe_5C_2(001) at 1 ML. Due to the small difference (<0.2 eV) in adsorption energy of **15** and **18**−**22** at high coverage, coexisting surface species of C_sH, C_sH_3, H_2, and H are possible, while C_sH_2 is not competitive. This agrees with the observation of CH_x ($x = 1-3$) fragments and C_sH_4 by infrared experiments during the processes of H_2-reduced iron carbide.[2]

On the basis of the calculated adsorption energies (Tables 1−3) on Fe_5C_2(001), it is shown that with increased surface coverage the adsorption energy decreases on one hand, and the coadsorption of other fragments becomes favorable on the other hand. Nevertheless, C_sH is the most stable fragment at all coverages.

3.1.2. Electronic Factor. Since the adsorption energies of **4** at 1/3 ML, **6**/**7** at 2/3 ML, and **15** at 1 ML on Fe_5C_2(001) with the C_sH fragment are very high, we only optimized the C_sH fragment in **4** at 1/3 ML, and examined the LDOS of C_sH and surface iron atoms as shown in Figure 6. The valence bands of isolated CH as a doublet ground state are shown as dashed lines. The occupied σ(CH) band is at about −9.8 eV, and the n(CH) (lone pair) band is at about −1.4 eV. The singly occupied p_x band is at −1.1 eV, and the empty (nonbonding) p_y and p_z bands are at around 0.3 and 2.2 eV, respectively, The σ*(CH) antibonding band lies at about 7.7 eV, which is out of the effective interaction range.[39]

After adsorption, all bands of C_sH shift downward. For example, the σ(CH) band shifts downward to about −12.0 eV, and the n(CH) band to about −6.3 eV, while the $p_{x,y,z}$ bands shift strongly in the range of −4.1 to −3.3 eV. In contrast to the p and d bands with less effect, the s band of Fe shifts downward relatively significantly. At the same energy level, there are new peaks in Fe s and p bands. This indicates the interaction of n(CH) and $p_{x,y,z}$ orbitals of C_sH with the s, p, and d orbitals of surface Fe.

In **5**, **9**−**11**, **16**, and **17** for H adsorption on Fe_5C_2(001) at 1/3, 2/3, and 1 ML, C_sH_2 is the most favored surface fragment,

TABLE 5: Computed Bond Lengths (*d*, Å) and Adsorption Energies (E_{ads}, eV) for Hydrogen Adsorption on Fe_5C_2(110) at 4/5 ML

	30	31	32	33	34	35	36	37	38	39
d_{H-H}	1.073		0.906							
d_{H-Fe}	1.538	1.657	1.643	1.684	1.690	1.661	1.721	1.694	1.954	
	1.568	1.693	1.662	1.737	1.748	1.686	1.754	1.876	1.729	
	1.990	1.658	1.717	1.877	1.892	1.894	1.828	1.895	1.786	
	1.623	1.725	1.806	1.672	1.694	1.694	1.667		1.834	
	1.715	1.786	1.824	1.681	1.699	1.709	1.852		1.810	
	1.641	1.657		1.669	1.907	1.696	1.863		1.949	
	1.735	1.753		1.824	1.697	1.731	1.739			
		1.721		1.835	1.699	1.960	1.943			
		1.734					1.928			
		1.868								
d_{H-Cs}			1.110	1.111	1.111	1.113	1.141	1.091	1.128	1.089
							1.213	1.101	1.132	1.089
								1.111	1.152	1.090
										1.095
E_{ads}	−0.86	−1.00	−0.82	−1.17	−0.99	−0.97	−0.71	−0.75	−0.58	−0.49
										(−0.03)[a]

[a] For CH_4 as absorbate.

TABLE 6: Computed Bond Lengths (*d*, Å) and Adsorption Energies (E_{ads}, eV) for Hydrogen Adsorption on Fe_5C_2(110) at 6/5 ML

	40	41	42	43	44	45	46
d_{H-H}	1.044						
d_{H-Fe}	1.546	1.822	1.825	1.750	1.704	1.736	1.703
	1.573	1.699	1.742	1.756	1.770	1.755	1.851
	1.608	1.718	1.744	1.823	1.870	1.861	1.759
	1.719	1.826	1.777	1.688	1.788	1.682	1.778
	1.673	1.669	1.658	1.691	1.791	1.825	1.829
	1.724	1.675	1.720		1.810	1.946	
	1.803	1.723	1.679				
	1.631	1.754	1.816				
	1.775	1.877	1.821				
			1.804				
d_{H-Cs}	1.108	1.090	1.113	1.088	1.089	1.089	1.088
		1.092	1.148	1.089	1.089	1.090	1.089
		1.140	1.153	1.090	1.089	1.090	1.090
				1.090	1.091	1.091	1.094
E_{ads}	−0.81	−0.73	−0.72	−0.82	−0.81	−0.79	−0.78
				(−0.01)[a]	(0.01)[a]	(0.01)[a]	(−0.03)[a]

[a] Using CH_4 as absorbate.

which is an important intermediate for the C−C coupling in FTS. We investigated the LDOS of the C_sH_2 fragment in **5** at 1/3 ML and isolated triplet ground state of the CH_2 diradical and Fe atoms in Figure 7. The occupied $\sigma(CH_2)$ band is in the range of −12.3 to −9.0 eV, and the $\pi(CH_2)$ band lies at −6.8 to −5.1 eV. The two singly occupied orbitals, $n(CH_2)$ and p_z, are at −2.8 to −1.3 eV and −0.7 eV, respectively. The antibonding $\sigma^*(CH_2)$ and $\pi^*(CH_2)$ bands are at 6.5 and 7.8 eV, respectively.[39]

After adsorption, all bands of C_sH_2 shift downward. For example, the $\sigma(C_sH_2)$ band is at −13.4 eV, and the $\pi(C_sH_2)$ band at −7.5 eV. The $n(CH_2)$ and p_z bands are at −6.4 eV, and small bands at −4.0 eV are broad. In contrast to the p and d bands, the s band of Fe shifts downward significantly. At the same energy level, there are new peaks in Fe s and p bands, indicating the interaction of $n(C_sH_2)$ and p_z orbitals of C_sH_2 with the s, p, and d orbitals of surface Fe.

For hydrogen adsorption on Fe_5C_2(001) at 2/3 ML, the adsorption energy of **12** with C_sH_3 at a 3-fold site is higher than that of **13** with C_sH_3 at an atop site. The LDOSs of C_sH_3 at atop and 3-fold sites are shown in Figure 8. For the valence molecular orbitals of CH_3, the fully occupied $\sigma(CH_3)$ band is at about −12.1 eV, and the $\pi(CH_3)$ band at −5.9 eV. The singly occupied n band is at about −1.6 eV. The $\sigma^*(CH_3)$ antibonding band is at 6.6 eV, and the $\pi^*(CH_3)$ antibonding band is high in energy at about 7.6 eV.[39]

After adsorption, at the atop site, there is a small shift in the $\sigma(C_sH_3)$ and $\pi(C_sH_3)$ bands, while at the 3-fold site, the $\sigma(C_sH_3)$ and $\pi(C_sH_3)$ band orbitals shift downward to about −13.6 and −6.8 eV, respectively. The n band is at −3.1 and −5.4 eV for atop and 3-fold sites; the band at the 3-fold site is broader than that at the atop site. At the same energy level, new peaks appear for both Fe s and p bands at atop and 3-fold sites. This stronger shift at the 3-fold site than at the atop site indicates the stronger interaction of C_sH_3 with surface iron at the 3-fold site than at the atop site, in line with the calculated adsorption energies. As a result, the C_sH_3 fragment preferentially binds in a 3-fold site on Fe_5C_2(001). This case also appears for the Ni surface in that Ni s and p orbitals are found to play important roles in CH_3 preferring adsorption at a 3-fold site on Ni(111).[40]

3.2. Hydrogen Adsorption on Fe_5C_2(110). *3.2.1. Adsorption Geometry*. As shown in Figure 9, there are six modes (**24**−**29**) for hydrogen adsorption on Fe_5C_2(110) at 2/5 ML, and the computed bond parameters and adsorption energies are given in Table 4. For hydrogen adsorption at atop (**24**) and 2-fold and 3-fold (**25**−**27**) sites, **24** has the lowest adsorption energy (−0.64 eV). In **24**, H_2 is strongly activated (H−H, 1.018 Å), but not dissociated, on Fe_5C_2(110). In contrast, **26** with hydrogen at 2-fold and 3-fold sites and **27** with H adsorbed at two 3-fold sites have the highest adsorption energies (−1.44 and −1.43 eV), respectively.

In **28** and **29**, surface C_sH is formed, but the adsorption energy of **28**/**29** is lower than that of **26**/**27**. In addition to C_sH, **28** and **29** also have H species at a 3-fold site and at a 2-fold site, respectively. Note that there is no stable surface C_sH_2 at 2/5 ML. Therefore, **26** and **27** are the most favored adsorption modes with atomic hydrogen on Fe_5C_2(110) at 2/5 ML.

For hydrogen adsorption on Fe_5C_2(110) at 4/5 ML, there are 10 adsorption modes (**30**−**39**), and the calculated bond parameters are given in Table 5 and Figure 10. **30** has strongly activated H_2 (H−H, 1.073 Å) and two 2-fold adsorbed H species, and **31** has two 2-fold and two 3-fold H species. As expected, **31** has higher adsorption energy than **30** (−1.00 vs −0.86 eV).

For **32**−**35**, surface C_sH is formed. Apart from that, **32** has activated H_2 (H−H, 0.906 Å) and one 3-fold H, while **33**−**35** have one 2-fold and two 3-fold H species. In **36**, surface C_sH_2 is formed, the C_s−H bond length is 1.141 and 1.213 Å, and one H of C_sH_2 is agostically bonded to an Fe atom at 1.739 Å.

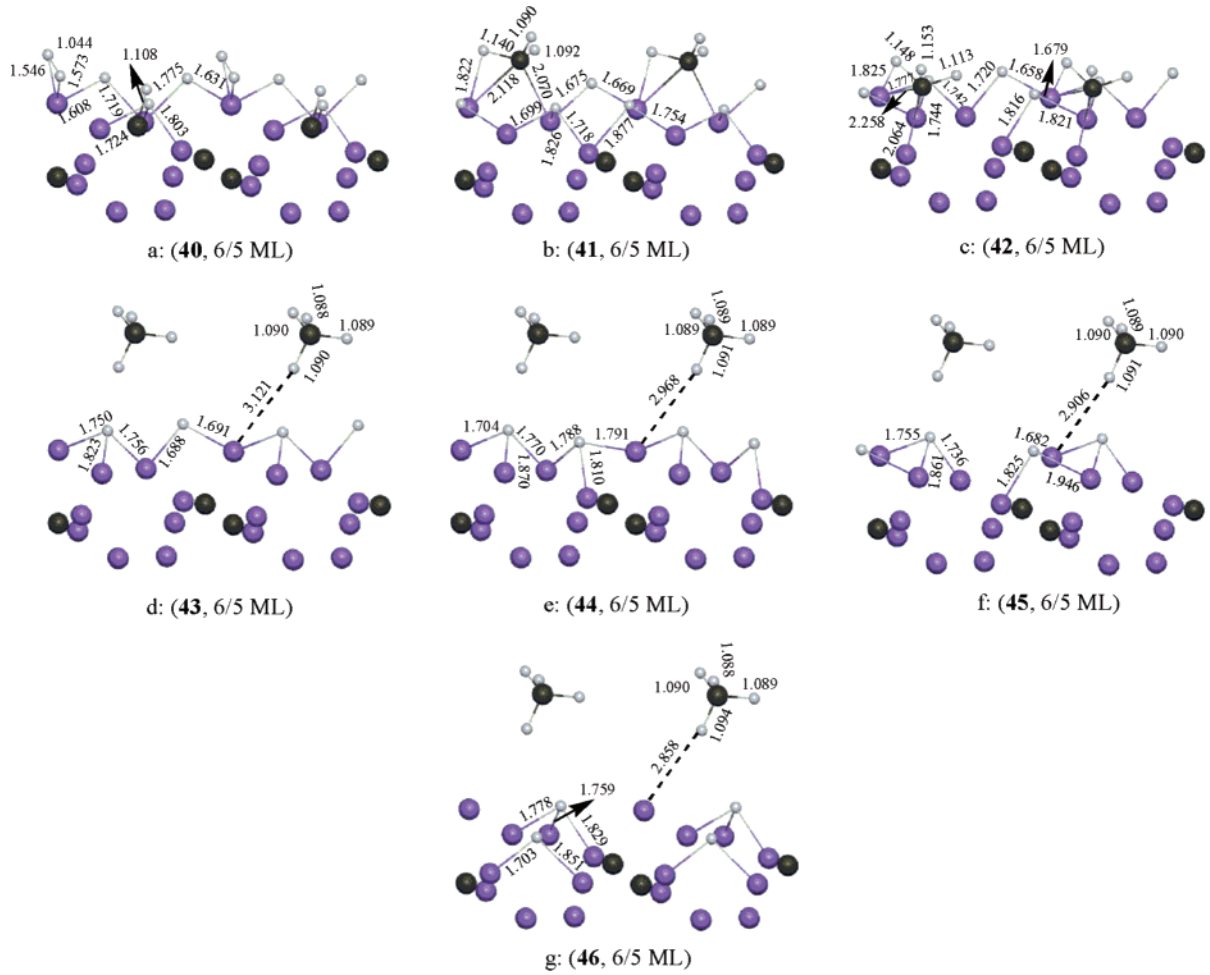

Figure 11. H adsorption on Fe_5C_2(110) at 6/5 ML (purple, Fe atom; gray, C atom; white, H atom).

In **37** and **38**, surface C_sH_3 is formed, **37** has a 2-fold C_sH_3 and one 3-fold H species, and **38** has a 3-fold C_sH_3 and a 3-fold H, respectively. Interestingly, one H of C_sH_3 in **38** is agostically bonded to Fe atoms at 1.810, 1.949, and 1.954 Å. On the basis of the adsorption energies (Table 5), the most favored mode on Fe_5C_2(110) at 4/5 ML is **33** with surface C_sH. This agrees with the experiments with CO/D_2 and $^{13}CO/H_2$ on Fe/Al_2O_3 during FTS.[4b]

The adsorption energy of **39** with surface C_sH_4 is the lowest among **30**−**39**. Considering CH_4 as adsorbate, the adsorption energy of CH_4 in **39** is only −0.03 eV. Therefore, no adsorbed CH_4 can exist on the surface.

For hydrogen adsorption on Fe_5C_2(110) at 6/5 ML, there are seven adsorption modes (**40**−**46**), and the calculated bond parameters are given in Table 6 and Figure 11. **40** has activated H_2 (H−H, 1.044 Å), two 2-fold H species, one 3-fold H species, and surface C_sH. Due to the high coverage, it is not possible to locate states with surface C_sH_2, and the next states are **41** and **42** with surface C_sH_3 in a 2-fold site and a 3-fold site, respectively. Apart from C_sH_3, **41** and **42** have one 2-fold and two 3-fold H species.

43−**46** are modes with C_sH_4, and there are one 2-fold H and one 3-fold H in **43** and **46**, and two 3-fold H species in **44** and **45**. Compared with **24**−**29** at 2/5 ML, H is adsorbed at deeper layer Fe atoms at 1.703 and 1.851 Å in **46** when the surface carbon atom is reduced to CH_4. Since **40**−**46** have nearly the same adsorption energies (Table 6), coexisting surface species of C_sH, C_sH_3, H_2, and H at 6/5 ML are possible. This agrees also with the observation of CH_x ($x = 1-3$) fragments and CH_4 by infrared experiments during the processes of H_2-reduced iron carbide.[2]

3.2.2. Electronic Factor. On Fe_5C_2(110) the adsorption energies of **28**/**29** at 2/5 ML, **32**−**35** at 4/5 ML, and **40** at 6/5 ML with C_sH fragments are generally high, and therefore, we optimized only the C_sH fragment in **28**, and examined the LDOS of C_sH and surface iron atoms as shown in Figure 12. Compared with the LDOS of a bare CH unit in Figure 6, the σ(CH) band shifts downward to about −11.9 eV, and the n(CH) band to about −6.7 eV, while the $p_{x,y,z}$ bands shift strongly in the range of −6.0 to −3.0 eV. In contrast to the p and d bands with less effect, the s band of Fe shifts downward relatively significantly. At the same energy level, there are new peaks in Fe s and p bands. This indicates the strong interaction of n(CH) and $p_{x,y,z}$ orbitals of C_sH with the s, p, and d orbitals of surface Fe.

In **37** and **41**, 2-fold C_sH_3 appears on Fe_5C_2(110) at 4/5 and 6/5 ML; therefore, we optimized only the C_sH_3 fragment in **37** and examined the LDOS as shown in Figure 13. Compared with the LDOS of a bare CH_3 unit in Figure 8, the 2-fold $\sigma(C_sH_3)$ orbital is at −13.1 eV, and the $\pi(C_sH_3)$ bands are at −6.2 eV. There is weak interaction between the σ and $\pi(C_sH_3)$ orbitals and the Fe s, p, and d orbitals. The n band is at −3.7 eV. At the same energy level, new peaks appear with both Fe s and p bands. This indicates the strong interaction of the n orbital with the s, p, and d orbitals of surface Fe.

3.3. Hydrogen Adsorption on Fe_5C_2(100). As shown in Figure 14, there are five modes (**47**−**51**) at 1/2 ML and two modes at 1 ML (**52**−**53**) for hydrogen adsorption on the "pure

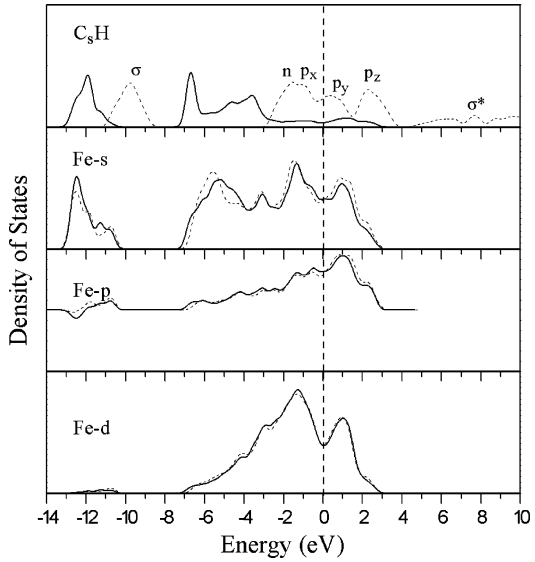

Figure 12. LDOS of the surface C_sH fragment in **28** at 2/5 ML on $Fe_5C_2(110)$ (solid line for bands after adsorption, dashed line for bands before adsorption).

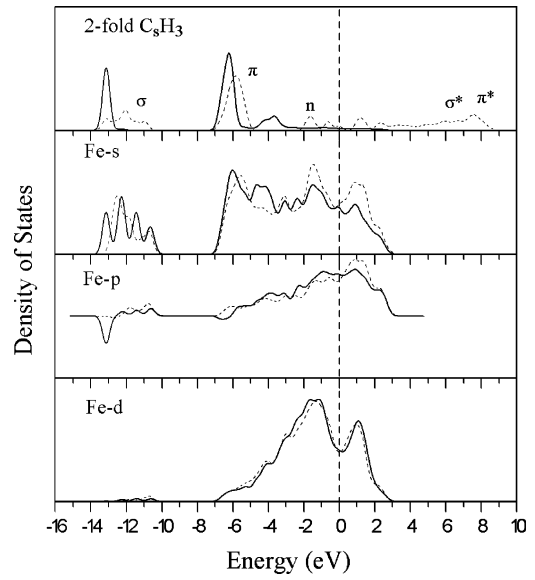

Figure 13. LDOS of the surface C_sH_3 fragment in **37** at 4/5 ML on $Fe_5C_2(110)$ (solid line for bands after adsorption, dashed line for bands before adsorption).

metal" surface $Fe_5C_2(100)$, and the computed bond parameters and adsorption energies are given in Table 7. As discussed above, the surface ML of $Fe_5C_2(100)$ does not have any carbon atoms, and therefore, only interaction between hydrogen and surface iron is possible.

For hydrogen adsorption at atop, 2-fold, and 3-fold sites (**47**−**51**), the adsorption energy of atop site **47** is the lowest (−0.82 eV). In **47**, H_2 is strongly activated, but not dissociated (H−H bond length, 1.036 Å). In **48**, which has the highest adsorption energy (−1.50 eV), H_2 is dissociated and adsorbed at 2-fold sites. However, the adsorption energy of species **51** with 3-fold H is lower than that of **48** with 2-fold H.

For H adsorption on $Fe_5C_2(100)$ at 1 ML, there are two modes (**52** and **53**). The adsorption energy of **52** is 0.23 eV higher than that of **53**. In **52**, there are two 2-fold and two 3-fold H species, while in **53**, there are one H_2 and two 3-fold H species. Consequently, dissociated H is favored at low and high coverage.

3.4. Discussion. At this point, we have conducted a detailed analysis of hydrogen adsorption on the (100), (001), and (110) surfaces of Fe_5C_2 by using DFT calculations. As shown in Figure 2, the top layer of $Fe_5C_2(100)$ consists originally only of iron atoms and therefore is metallic in character, and the first carbon layer covered by the first iron layer is not active for H_2 adsorption. For (001) and (110), the surfaces consist of both iron and carbon atoms, but they differ in the surface structure and composition. For example, (001) has the carbon layer on the top, while (110) has the carbon layer exposed under the first iron layer. Therefore, both surfaces have similarities and differences in H_2 adsorption. At high coverage, for example, both surfaces are similar in H_2 adsorption, but different at low coverage. C_sH is the major species at 1/3 ML on (001), while H is the major surface species at 2/5 ML on (110). C_sH and C_sH_2 are the major surface species at 2/3 ML on (001), while C_sH and H are the major surface species at 4/5 ML on (110). The formation of these surface species shows the differences in surface activities and selectivities, which are essential for chain growth and the product spectrum in the FTS process.

Apart from the most stable CH species, however, note that other less stable species (CH_2 and CH_3) may also be more important for FTS by taking the dynamic situation into account. This is because too strong adhesion of surface sites and adsorbed species can suppress the kinetics and dynamics of the FTS process. On the other hand, there is also a possibility for CO activation and dissociation on the less stable adsorbed site due to a smaller barrier than on the most stable adsorbed site.[41] In these cases, this implies a kinetic and thermodynamic equilibrium between different adsorption sites. Interestingly, our DFT results have clearly reproduced the common point in FTS; i.e., methane can be quite easily formed on the surface with a bit high static energy and immediately leaves the surfaces as imaged on the basis of the static results. In summary, on these two surfaces containing carbon atoms, FTS occurs once an activated hydrogen environment is available. Along with the formation of C_xH_y surface species, deep reduction of carbon-containing surfaces can form a metal-rich or pure metallic surface, which might be similar to (100). This implies the possibility of phase transfer. In turn, once CO is adsorbed, the (100) surface can also be converted to carbon-containing surfaces by CO dissociation, which are similar to (001) and (110). Thus, the understanding of the reaction mechanisms or the elementary steps under the changes of surface structures and composition will be interesting and exciting aspects for future work.

Among the formed phases, the Fe_5C_2 phase has been proved to be the most important active phase, and correlates with FTS activity significantly.[31] The complexity of iron-based FTS catalysis is mainly attributed to the coexistence and coaction of all phases detected in working catalysts. During FTS, a syngas ($CO + H_2$) imposes a significant influence on the catalyst surface: (1) CO adsorption on the surface of Fe_5C_2[27] results in the formation of surface carbon species and the reduction and carburization of the iron phase. (2) H_2 adsorption on the surface results in the reduction of the surface and the formation of C_xH_y species essential for the formation of hydrocarbons. (3) Coaction of syngas on the surface causes the complex and dynamic situation of the surface structures and composition. The catalytic cycle can be completed and propagated by a continuous supply of syngas.[42]

With these basic facts in mind, the results on this work together with the previous DFT calculations for CO adsorption

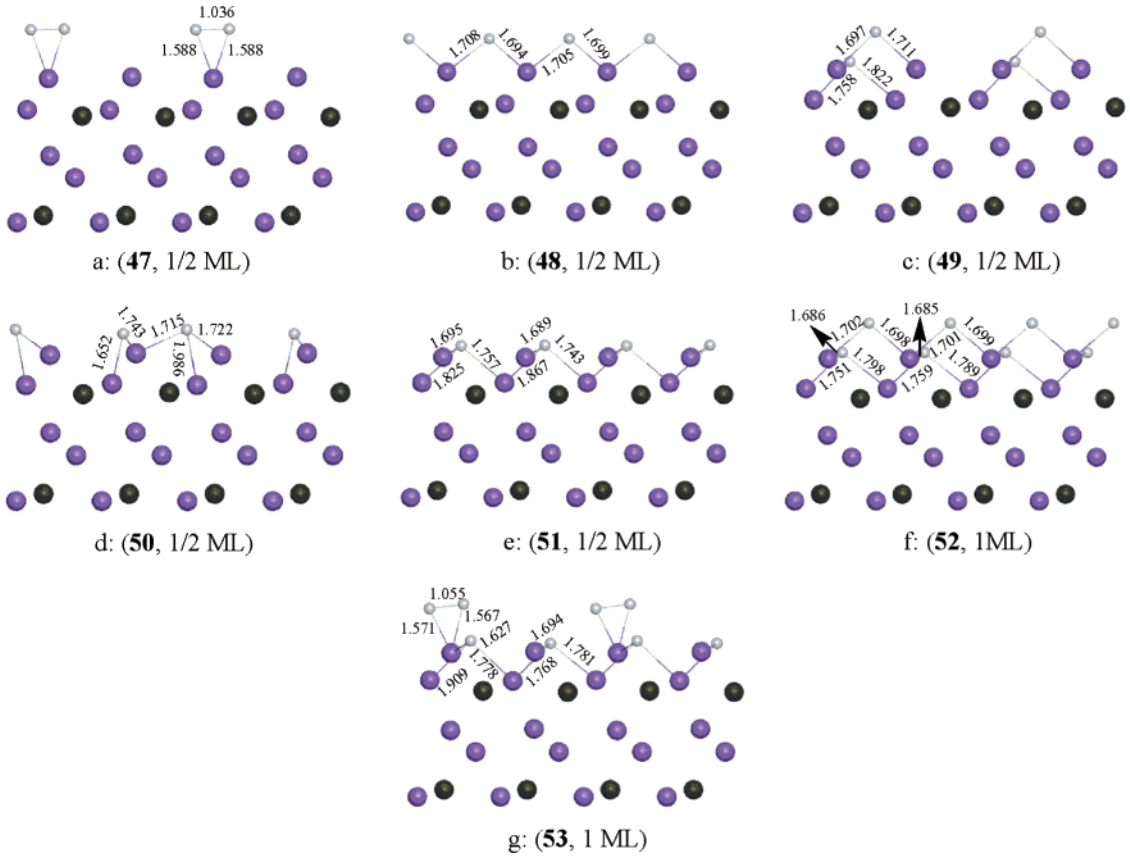

Figure 14. H adsorption on Fe_5C_2(100) (purple, Fe atom; gray, C atom; white, H atom).

TABLE 7: Computed Bond Lengths (*d*, Å) and Adsorption Energies (E_{ads}, eV) for Various Coverages (ML) of Hydrogen Adsorption on Fe_5C_2(100)[a]

	47, 1/2	**48**, 1/2	**49**, 1/2	**50**, 1/2	**51**, 1/2	**52**, 1	**53**, 1
d_{H-H}	1.036						1.055
d_{H-Fe}	1.588	1.694	1.697	1.652	1.695	1.686	1.567
	1.588	1.708	1.711	1.743	1.757	1.751	1.571
		1.699	1.689	1.715	1.825	1.798	1.627
		1.705	1.758	1.722	1.689	1.698	1.778
			1.822	1.986	1.743	1.702	1.909
					1.867	1.685	1.694
						1.759	1.768
						1.789	1.781
						1.699	
						1.701	
E_{ads}	−0.82	−1.50	−1.16	−1.05	−0.98	−1.12	−0.89

[a] The coverage is given in the column heads following the species number.

on Fe_5C_2(001), -(110), and -(100) have brought forth the FTS nature. All Fe_5C_2 surfaces may play essential roles resulting from CO adsorption,[27] and the metallic (100) surface may provide energetically more favorable sites for CO deposition, especially at high CO coverage corresponding to the typical FTS environment. However, CO activation is relatively weaker compared to that of the other two surfaces, (001) and (110), if only CO is present in the system. Our current results show that H_2 adsorption on (100) provides an energetically more favorable site for H_2 dissociation. The dissociated hydrogen might play different roles in a dynamic FTS situation. The possible (perhaps most important) roles may relate to the further activation of deposited CO on this surface, and FTS might also take place on this surface although no surface species essential for FTS were directly formed for the separated consideration of H_2 and CO adsorption.

4. Conclusion

Our present DFT results provide an informative picture for H adsorption on the (001), (110), and (100) surfaces of Fe_5C_2. For H adsorption on Fe_5C_2(001) at 1/3 ML, the most stable surface fragments are C_sH and H at a 3-fold site, and other species (H_2 and C_sH_2) are not competitive. Due to this low coverage, formation of C_sH_3 and C_sH_4 is not possible. With increased surface coverage, other surface hydrocarbon fragments become possible, as indicated at 2/3 ML, but C_sH is still the most favored surface fragment, followed by C_sH_2. At full coverage (1 ML), formation of C_sH_4 is more favored thermodynamically, and both C_sH and C_sH_3 have nearly the same adsorption energies.

For H adsorption on Fe_5C_2(110) at 2/5 ML, atomic hydrogen is preferred to adsorption at a 2-fold site and a 3-fold site, other species (H_2 and C_sH) are not competitive, and no stable C_sH_2 can be found. This is similar to the results for Fe_5C_2(001) at 1/3 ML. At 4/5 ML, however, C_sH becomes the most stable fragment, and the formation of C_sH_2, C_sH_3, and C_sH_4 is not competitive. It is found that coexistence and coadsorption of C_sH, C_sH_3, and C_sH_4 are possible at 6/5 ML according to their adsorption energies, and no stable C_sH_2 can be found. For hydrogen adsorption on the (001) and (110) surfaces, similarities in containing carbon atoms on these two surfaces have led to the formation of CH_x ($x = 1-3$) species essential for FTS.

Due to a lack of surface carbon atoms on a monolayer on Fe_5C_2(100), H_2 prefers to be dissociated at low and high coverage. The different distribution of surface species results from the activity and selectivity of different adsorption sites. Although the equilibrium distribution of surface species CH_x ($x = 1-3$), CH_4, H_2, and H is governed thermodynamically, their rates of accumulation on the surfaces are determined by the corresponding kinetic parameters. The activation barriers

for the reaction of surface carbon atoms reducing to CH_x ($x = 1-4$) will be investigated in the future. The most interesting and exciting aspects of theoretical studies are the understanding of the changes of the surface structures and compositions under the real reaction conditions of FTS, and this in turn gives insight into the detailed reaction mechanisms.

Acknowledgment. We thank the Key Project of the Chinese Academy of Sciences and the 863 Project of the Ministry of Science and Technology of China (Grant Nos. 2001AA523010 and KGC X1-SW-02) and the National Natural Science Foundation of China (Grants No. 20473111 and No. 20590360) for financial support.

References and Notes

(1) (a) Datye, A. K.; Jin, Y. M.; Mansker, L.; Motjope, R. T.; Dlamini, T. H.; Coville, N. J. *Stud. Surf. Sci. Catal.* **2000**, *130B*, 1139. (b) Jin, Y. M.; Mansker, L.; Datye, A. K. *Prepr.—Am. Chem. Soc., Div. Pet. Chem.* **1999**, *44*, 97. (c) Bartholomew, C. H.; Stoker, M. W.; Mansker, L. Datye, A. K. *Stud. Surf. Sci. Catal.* **1999**, *126*, 265. (d) Zhang, Y. Q.; O'Brien, R. J.; Davis, B. H.; Hamdeh, H. H. *Prepr.—Am. Chem. Soc., Div. Pet. Chem.* **1999**, *44*, 100. (e) Jin, Y. M.; Datye, A. K. *Stud. Surf. Sci. Catal.* **1998**, *119*, 209. (f) Davis, B. H. *Catal. Today* **2003**, *84*, 83. (g) O'Brien, R. J.; Xu, L. G.; Spicer, R. L.; Davis, B. H. *Energy Fuels* **1996**, *10*, 921. (h) Rao, K. R. P. M.; Huggins, F. E.; Mahajan, V.; Huffman, G. P.; Burkur, D. B.; Rao, V. U. S. *Hyperfine Interact.* **1994**, *93*, 1751.

(2) (a) Bian, G. Z.; Oonuki, A.; Kobayashi, Y.; Koizumi, N.; Yamada, M. *Appl. Catal., A* **2001**, *219*, 13. (b) Bian, G. Z.; Oonuki, A.; Koizumi, N.; Nomoto, H.; Yamada, M. *J. Mol. Catal. A* **2002**, *186*, 203.

(3) (a) Bent, B. E. *Chem. Rev.* **1996**, *96*, 1361. (b) Davis. S. M.; Somorjai, G. A. In *The Chemical Physics of Solid Surfaces and Heterogeneous Catalysis*; King, D. A., Woodruff, D. P., Eds.; Elsevier: Amsterdam, 1982; Vol. 4, p 217. (c) Schulz, H. *Appl. Catal., A* **1999**, *186*, 3. (d) Herrmann, W. A. *Angew. Chem., Int. Ed. Engl.* **1982**, *21*, 117.

(4) (a) Deng, B.; Campbell, T. J.; Burris, D. R. *Environ. Sci. Technol.* **1997**, *31*, 1185. (b) Stockwell, D. M.; Bianchi, D.; Bennett, C. O. *J. Catal.* **1988**, *113*, 13.

(5) Christmann, K. *Surf. Sci. Rep.* **1988**, *9*, 1.

(6) Anderson, R. B. *The Fischer-Tropsch Reaction*; Academic Press: London, U.K., 1984.

(7) Myers, S. M.; Baskes, M. I.; Birnbaum, H. K.; Corbett, J. W.; De Leo, G. G.; Estreicher, S. K.; Haller, E. E.; Jena., P. N.; Johnson, N. M.; Kirchheim, R.; Pearton, S. J.; Stavola, M. J. *Rev. Mod. Phys.* **1992**, *64*, 559.

(8) Jiang, D. E.; Carter, E. A. *Surf. Sci.* **2003**, *547*, 85.

(9) Paul. J. F.; Sautet, P. *Surf. Sci. Lett.* **1996**, *356*, L403.

(10) Ciobîcă, I. M.; Kleyn, A. W.; van Santen, R. A. *J. Phys. Chem. B* **2003**, *107*, 164.

(11) Kinke, D. J., II; Broadbelt, L. J. *Surf. Sci.* **1999**, *429*, 169.

(12) Bradshaw, A. M.; van der Veen, F. J.; Himpsel, F. J.; Eastman, D. E. *Solid State Commun.* **1981**, *37*, 37.

(13) Aizawa, T.; Hayami, W.; Souda, R.; Otani, S.; Ishizawa, Y. *Surf. Sci.* **1997**, *381*, 157.

(14) Ciobîcă, I. M.; Frechard, F.; van Santen, R. A.; Kleyn, A. W.; Hafner, J. *Chem. Phys. Lett.* **1999**, *311*, 185.

(15) (a) Wu, M.-C.; Goodman, D. W. *J. Am. Chem. Soc.* **1994**, *116*, 1364. (b) Wu, M.-C.; Goodman, D. W. *Surf. Sci. Lett.* **1994**, *306*, L529.

(16) Petersen, M. A.; Jenkins, S. J.; King, D. A. *J. Phys. Chem. B* **2004**, *108*, 5909.

(17) Watson, D. T. P.; Titmuss, S.; King, D. A. *Surf. Sci.* **2002**, *505*, 49.

(18) White, J. A.; Bird, D. M. *Phys. Rev. B* **1994**, *50*, 4954.

(19) (a) Payne, M. C.; Allan, D. C.; Arias, T. A.; Joannopoulos, J. D. *Rev. Mod. Phys.* **1992**, *64*, 1045. (b) Milman, V.; Winkler, B.; White, J. A.; Pickard, C. J.; Payne, M. C.; Akhmataskaya, E. V.; Nobes, R. H. *Int. J. Quantum Chem.* **2000**, *77*, 895.

(20) Vanderbilt, D. *Phys. Rev. B* **1990**, *41*, 7892.

(21) Monkhorst, H. J.; Pack, J. D. *Phys. Rev. B* **1976**, *13*, 5188.

(22) Louie, S. G.; Froyen, S.; Cohen, M. L. *Phys. Rev. B* **1982**, *26*, 1738.

(23) (a) Nayak, S. K.; Nooijen, M.; Bernasek, S. L. *J. Phys. Chem. B* **2001**, *105*, 164. (b) Cheng, H. S.; Reiser, D. B.; Dean, S. W., Jr.; Baumert, K. *J. Phys. Chem. B* **2001**, *105*, 12547. (c) Ge, Q.; Jenkins, S. J.; King, D. A. *Chem. Phys. Lett.* **2000**, *327*, 125.

(24) Le Caer, G.; Simon, A.; Lorenzo, A.; Genin, J. M. *Phys. Status Solidi A* **1971**, *6*, K97.

(25) Immel, S. *Molarch*$^+$, *MOLecular ARCHlitecture Modeling Programm V7.05*; Technical University of Darmstadt: Darmstadt, Germany, 2002.

(26) Jack, K. H.; Wild, S. A. *Acta Crystallogr.* **1966**, *S 21*, A81.

(27) Cao, D.-B.; Zhang, F.-Q.; Li, Y.-W.; Jiao, H. *J. Phys. Chem. B* **2004**, *108*, 9094.

(28) Shroff, M. D.; Kalakkad, D. S.; Coulter, K. E.; Köhler, S. D.; Harrington, M. S.; Jackson, N. B.; Sault, A. G.: Daye, A. K. *J. Catal.* **1995**, *156*, 185.

(29) Pham, H. N.; Datye, A. K. *Catal. Today* **2000**, *58*, 233.

(30) Jin, Y.; Datye, A. K. *J. Catal.* **2000**, *196*, 8.

(31) Yang, Y.; Xiang, H. W.; Xu, Y. Y.; Bai, L.; Li, Y. W. *Appl. Catal., A* **2004**, *266*, 181.

(32) Moritz, W.; Imbihl, R.; Behm, R. J.; Ertl, G.; Matsushima, T. *J. Chem. Phys.* **1985**, *83*, 1959.

(33) Kinke, D. J., II; Dooling, D. J.; Broadbelt, L. J. *Surf. Sci.* **1999**, *425*, 334.

(34) Ge, Q.; Neurock, M.; Wright, H. A.; Srinivasan, N. *J. Phys. Chem. B* **2002**, *106*, 2826.

(35) Zheng, C.; Apeloig, Y.; Hoffmann, R. *J. Am. Chem. Soc.* **1988**, *110*, 749.

(36) Minot, C.; van Hove, M. A.; Somirjai, G. A. *Surf. Sci.* **1982**, *127*, 441.

(37) (a) Yang, Q. Y.; Maynard, K. J.; Johnson, A. D.; Ceyer, S. T. *J. Chem. Phys.* **1995**, *102*, 7734. (b) Kratzer, P.; Hammer, B.; Nørskov, J. K. *J. Chem. Phys.* **1996**, *105*, 5595. (c) Burghgraef, H.; Jansen, A. P. J.; van Santen, R. A. *Chem. Phys.* **1993**, *177*, 407. (d) Schüle, J.; Siegbahn, P.; Wahlgren, U. *J. Chem. Phys.* **1988**, *89*, 6982. (e) Yang, H.; Whitten, J. L. *J. Am. Chem. Soc.* **1991**, *113*, 6442.

(38) (a) Au, C.-T.; Liao, M.-S.; Ng, C.-F. *J. Phys. Chem. A* **1998**, *102*, 3959. (b) Michaelides, A.; Hu, P. *J. Chem. Phys.* **2001**, *114*, 2523.

(39) For the construction and discussion of orbitals, see: Jorgensen, W. L.; Salem, L. *The Organic Chemist's Book on Orbitals*; Academic Press: New York, 1973.

(40) Papoian, G.; Nørskov, J. K.; Hoffmann, R. *J. Am. Chem. Soc.* **2000**, *122*, 4129.

(41) Gong, X. Q.; Raval, R.; Hu, P. *Surf. Sci.* **2004**, *562*, 247.

(42) Sudsakorn, K.; Goodwin, J. G., Jr.; Adeyiga, A. A. *J. Catal.* **2003**, *213*, 204.